AD

TECHNICAL REPORT ARLCB-TR-81008

A PHOTOELASTIC STUDY OF STRESSES IN SINGLE-GROOVE CONNECTIONS OF THE SAME MATERIAL

Y. F. Cheng

February 1981

US ARMY ARMAMENT RESEARCH AND DEVELOPMENT COMMAND
LARGE CALIBER WEAPON SYSTEMS LABORATORY
BENÉT WEAPONS LABORATORY
WATERVLIET, N. Y. 12189

AMCMS No. 6111.01.91A0

PRON No. 1A1281501A1A

DISCLAIMER

The findings in this report are not to be construed as an official Department of the Army position unless so designated by other authorized documents.

The use of trade name(s) and/or manufacturer(s) does not constitute an official indorsement or approval.

DISPOSITION

Destroy this report when it is no longer needed. Do not return it to the originator.

SECURITY CLASSIFICATION OF THIS PAGE *(When Data Entered)*

REPORT DOCUMENTATION PAGE

READ INSTRUCTIONS BEFORE COMPLETING FORM

1. REPORT NUMBER: ARLCB-TR-81008	2. GOVT ACCESSION NO.
3. RECIPIENT'S CATALOG NUMBER	
4. TITLE *(and Subtitle)*: A PHOTOELASTIC STUDY OF STRESSES IN SINGLE-GROOVE CONNECTIONS OF THE SAME MATERIAL	5. TYPE OF REPORT & PERIOD COVERED
	6. PERFORMING ORG. REPORT NUMBER
7. AUTHOR(s): Y. F. Cheng	8. CONTRACT OR GRANT NUMBER(s)
9. PERFORMING ORGANIZATION NAME AND ADDRESS: US Army Armament Research and Development Command, Benet Weapons Laboratory, DRDAR-LCB-TL, Watervliet, NY 12189	10. PROGRAM ELEMENT, PROJECT, TASK AREA & WORK UNIT NUMBERS: AMCMS No. 6111.01.91A0, PRON No. 1A1281501A1A
11. CONTROLLING OFFICE NAME AND ADDRESS: US Army Armament Research and Development Command, Large Caliber Weapon Systems Laboratory, Dover, NJ 07801	12. REPORT DATE: February 1981
	13. NUMBER OF PAGES: 30
14. MONITORING AGENCY NAME & ADDRESS *(if different from Controlling Office)*	15. SECURITY CLASS. *(of this report)*: UNCLASSIFIED
	15a. DECLASSIFICATION/DOWNGRADING SCHEDULE

16. DISTRIBUTION STATEMENT *(of this Report)*

Approved for public release; distribution unlimited.

17. DISTRIBUTION STATEMENT *(of the abstract entered in Block 20, if different from Report)*

18. SUPPLEMENTARY NOTES

19. KEY WORDS *(Continue on reverse side if necessary and identify by block number)*

Groove Connections
Photoelasticity
Maximum Fillet Stresses
Contact Stresses
Stress Concentrations

20. ABSTRACT *(Continue on reverse side if necessary and identify by block number)*

This report describes a three-dimensional photoelastic study on stresses in single-groove connections of the same material. Two groove profiles were investigated; namely, the British standard buttress and the new profile. Boundary stresses, interior stresses, and contact stresses were determined. Shear-difference method was used and the procedure of the method was outlined.

(CONT'D ON REVERSE)

DD FORM 1 JAN 73 1473 EDITION OF 1 NOV 65 IS OBSOLETE

UNCLASSIFIED

SECURITY CLASSIFICATION OF THIS PAGE *(When Data Entered)*

20. Abstract (Cont'd)

Appropriate checks for the accuracy of the results were made. Heywood's empirical equation for calculating maximum fillet stress in loaded projections was reviewed. It was found that the British standard buttress is stronger than the new profile and that the Heywood's equation is not applicable in our problem. Further work on multi-groove connection is in progress.

TABLE OF CONTENTS

Page

TABLES

LIST OF ILLUSTRATIONS

ACKNOWLEDGMENT

Charles Cobb's participation in the experimental phase of this investigation is hereby acknowledged.

INTRODUCTION

The practical motivation for the present investigation arose out of a study of critical stresses at the core of kinetic energy penetrators. In a kinetic energy penetrator, the core and the sabot are in contact through a series of circumferential grooves where the forward thrust is transmitted. Recently, the core of a penetrator with British standard buttress grooves failed transversely during a test. The failure was originated at the fillet of the first groove indicating the presence of a high tensile boundary stress. The objectives of this investigation were to determine the maximum boundary stress on the fillet of the groove and the distribution of contact stresses. In addition, stress distributions along the narrowest section of the core were determined to provide an equilibrium check for the accuracy of the results. Two groove profiles were studied; namely, the British standard buttress, Figure 1, and a new profile, Figure 2. All data was obtained photoelastically by means of the three-dimensional shear-difference method in combination with stress-freezing-and-slicing techniques. For the first model (British standard buttress profile), comparisons were made between experimental results and those calculated from Heywood's empirical equation.[1] No comparisons were made for the second model (new profile).

In a kinetic energy penetrator, the core and the sabot are usually made of different materials and consist of a series of grooves. However, the preliminary investigation reported here is confined to single-groove connections of same materials. Further work on multi-groove connections is in progress

---

[1]Heywood, R. B., "Tensile Fillet Stresses in Loaded Projections," Proceedings of the Institute of Mechanical Engineers, Vol. 159, pp. 384-391, 1948.

and will be reported at a later date.

EXPERIMENTAL PROCEDURE

Construction and Loading of Model

Two models of single-groove connection were constructed of photoelastic material PLM4B, supplied by MEASUREMENT GROUP, Raleigh, NC. Figure 3 shows a sketch of the first model with British standard buttress groove profile. The groove in the second model had a new profile as shown in Figure 2. For the convenience of taking data and the conservation of material, the groove in the model was scaled up eight times from the prototype while the pitch diameter only 2.72 times. The scaling difference has no effect on the stresses in the vicinity of the groove. The outer piece (sabot) consisted of two semi-cylinders. They were cemented together after assembly. Dowel pins made of the same photoelastic material were used to assure perfect alignment.

The model was loaded in a stress-frozen furnace by means of dead weights. The loaded model and the calibration disks were slowly heated to the critical temperature of 250°F, which was held constant for eight hours, and then gradually cooled to room temperature at which time the loads were removed. The rate of heating was 10°F/hour, and the rate of cooling 1°F/hour. The duration of the cycle was about eight-nine days. The loads were 59.1 pounds and 58.8 pounds for the first and second models, respectively, including the body weight of the outer piece.

Slicing Plan

One meridian slice was removed from the core and outer piece of each model for photoelastic observations. Its thickness was 0.1 inch. The plane of the slice was 90 degrees from the cement joint.

Scope of Investigation

The tangential free boundary stresses along the fillet of the groove were measured and contact stresses were found. In addition, stress distributions along the narrowest cross section in the core were determined. These will be described later.

Precision of Measurements

The photoelastic data, i.e., the fringe orders and isoclinic parameters, were measured by means of a photometer (Photovolt Corporation, Model 520M) and a precision polariscope specially designed for three-dimensional analysis. The photometer detected the minimum light intensity. The polariscope had a super-pressure compact mercury arc (OSRAM) as its light source. The combination of a condensing lens, a pin hole, a collimating lens, and a monochromatic filter provided a field of collimated monochromatic light of 5461 Å where the slice was placed. A pair of Glan-Thompson prisms were used as the polarizer and analyzer. They were mechanically coupled with a quarter-wave plate. Fractional fringe orders were measured by means of Senarmont's principle of compensation[2,3] with errors not exceeding ± 0.005

---

[2]Jessop, H. T. and Harris, F. C., "Photoelasticity - Principle and Methods," p. 176, Dover Publications, Inc., New York, 1949.

[3]Cheng, Y. F., "Some New Techniques for Scattered Light Photoelasticity," Experimental Mechanics, Vol. 3, No. 11, pp. 275-278, Nov. 1963.

fringes. The error in isoclinics did not exceed ± 1 degree. A lens projected a 5X image of stress pattern of the slice onto a screen in front of the photomultiplier tube. The screen had an 0.03 inch pin hole and gave a resolution of 0.006 inch in the slice.

Three-Dimensional Shear-Difference Sub-Slice Method

The three-dimensional shear-difference sub-slice method was developed by Frocht and Guernsey[4,5] in 1952. For the sake of completeness of this report, a brief outline is given here. The necessary and sufficient photoelastic data, i.e., the fringe orders and isoclinic parameters, for the complete determination of stresses along a given line are obtained from a sub-slice having the form of a parallelopiped, the axis of which is the given line of interest, Figure 4(a). The shearing stresses τ_{yx} and τ_{zx} on the four longitudinal sides, Figure 4(b), are determined from four observations at normal incidence: L_1, L_3, L_4, and L_6. For example,

$$\tau_{yx} = \frac{1}{2}(p'-q')\sin 2\phi' \qquad (1)$$

---

[4]Frocht, M. M. and Guernsey, R. Jr., "Studies in Three-Dimensional Photoelasticity - The Application of the Shear-Difference Method to the General Space Problem," Proceedings First US National Congress of Applied Mechanics, pp. 301-307, December 1952.

[5]Frocht, M. M. and Guernsey, R. Jr., "Further Work on the General Three-Dimensional Photoelastic Problem," Journal of Applied Mechanics, Trans. ASME, Vol. 77, No. 2, pp. 183-189, June 1955.

where p' and q' are the secondary principal stresses* at a point in the xy-plane obtained from normal incidence in the z-direction, and ϕ' is the corresponding isoclinic parameter. Similarly

$$\tau_{zx} = \frac{1}{2}(p''-q'')\sin 2\phi'' \tag{2}$$

where p" and q" are the secondary principal stresses at a point in the xz-plane obtained from normal incidence in the y-direction, and ϕ'' is the corresponding isoclinic parameter. Knowing τ_{yx} and τ_{zx}, it is possible to determine an approximation to the partial derivatives $\partial\tau_{yx}/\partial y$ and $\partial\tau_{zx}/\partial z$. Thus

$$(\partial\tau_{yx}/\partial y)_{x,y,z} \simeq (\Delta\tau_{yx}/\Delta y)_{x,y,z}$$

$$= [(\tau_{yx})_{x,y+(\Delta y/2),z} - (\tau_{yx})_{x,y-(\Delta y/2),z}]/\Delta y \tag{3a}$$

$$(\partial\tau_{zx}/\partial z)_{x,y,z} \simeq (\Delta\tau_{zx}/\Delta z)_{x,y,z}$$

$$= [(\tau_{zx})_{x,y,z+(\Delta z/2)} - (\tau_{zx})_{x,y,z-(\Delta z/2)}]/\Delta z \tag{3b}$$

where the subscripts denote the coordinates of the points where the shears are evaluated.

*The secondary principal stresses for a given direction are the principal stresses resulting from the stress components which lie in a plane normal to the direction. Thus the secondary principal stresses p' and q' for the z-direction are the principal stresses resulting from the stress components σ_x, σ_y and τ_{xy} and $p',q' = (1/2)(\sigma_x+\sigma_y) \pm \{[(1/2)(\sigma_x-\sigma_y)]^2 + \tau_{xy}^2\}^{1/2}$. The other stress components which lie in a plane parallel to the given direction have no photoelastic effect when observed along the direction.

Knowing $\Delta\tau_{xy}/\Delta y$ and $\Delta\tau_{zx}/\Delta z$, it is possible to determine approximately the stress σ_x at any point on the x-axis, i.e., the line of interest. From the first differential equation of equilibrium without body forces

$$\partial\sigma_x/\partial x + \partial\tau_{yx}/\partial y + \partial\tau_{zx}/\partial z = 0 \tag{4}$$

we obtain, upon integration and substitution of finite differences, the expression

$$(\sigma_x)_i = (\sigma_x)_o - \sum_o^i (\Delta\tau_{yx}/\Delta y)\Delta x - \sum_o^i (\Delta\tau_{zx}/\Delta z)\Delta x \tag{5}$$

where the subscript o denotes the starting point at the boundary having a known initial value of σ_x and the subscript i denotes any interior point on the axis.

Once $(\sigma_x)_i$ is known, the remaining normal stresses $(\sigma_y)_i$ and $(\sigma_z)_i$ can be computed from the following equations:

$$(\sigma_y)_i = (\sigma_x)_i - (p'-q')\cos 2\phi' \tag{6a}$$

$$(\sigma_z)_i = (\sigma_x)_i - (p''-q'')\cos 2\phi'' \tag{6b}$$

The remaining shearing stress τ_{yz} can be determined from an observation at oblique incidence: L_θ, Figure 4(a) and is given by the equation

$$\tau_{yz} = (F_\theta n_\theta \sin 2\phi_\theta - \tau_{yx}\cos\theta)\csc\theta \tag{7}$$

where θ is the angle of incidence of the oblique ray L_θ, F_θ the model fringe value in shear, ϕ_θ the isoclinic parameter, and n_θ the fringe order for the oblique path.

EXPERIMENTAL RESULTS

Fillet Boundary Stresses

Figures 5(a) and 5(b) show the stress patterns of meridian slices from the first and second models, respectively. It can be seen that in both models the fringe orders at the free fillet boundary in the outer piece are considerably less than those in the core. On the free boundary one of the principal stresses is identically zero, and the remaining principal stress tangent to the boundary is given by the fringe order. Figures 6(a) and 6(b) show the free fillet boundary stress, σ_f, in the core of the first and second models, respectively. In the first model, the boundary stress has a maximum value of $(\sigma_f)_{max} = 61$ psi and is located approximately 21 degrees from the narrowest section, measured toward the loaded surface. In the second model, $(\sigma_f)_{max}$ has a value of 98 psi and is located approximately 43 degrees from the narrowest section, measured toward the loaded surface. This value is almost 60 percent greater than that of the first model while their loads are practically the same.

Radial Distribution of Stresses σ_r, σ_z, and τ_{rz} on the Narrowest Section of the Core

In a $r\theta z$-cylindrical coordinate system, equation (5) takes the following form

$$(\sigma_r)_i = (\sigma_r)_o - \sum_o^i (\Delta\tau_{zr}/\Delta z)\Delta r - \sum_o^i (\Delta\tau_{\theta r}/\Delta\theta)\Delta r \qquad (8)$$

For an axially symmetric problem, $\tau_{\theta r} \equiv \tau_{\theta z} \equiv 0$, equation (8) reduces to

$$(\sigma_r)_i = (\sigma_r)_o - \sum_o^i (\Delta\tau_{zr}/\Delta z)\Delta r \qquad (9)$$

where $(\sigma_r)_o$ is the value of σ_r at the starting point, and τ_{zr} is obtained by making photoelastic observations of the meridian slice at normal incidence to the rz-plane. Once $(\sigma_r)_i$ is known, $(\sigma_z)_i$ can be computed from photoelastic relations similar to equation (6).

For a complete determination of the state of stress, the remaining normal stress σ_θ can be obtained by preparing a sub-slice from the meridian slice. This sub-slice has the form of a parallelopiped and its axis is the given line of interest, the radial line. An observation at normal incidence to the $r\theta$-plane along the z-direction, together with a photoelastic relation similar to equation (6), yields the normal stress σ_θ. However, due to the interest of preserving the meridian slices, the sub-slice has not been prepared and σ_θ has not been determined.

Figures 7(a) and 7(b) show the radial distribution of stresses σ_r, σ_z, and τ_{rz} on the narrowest section of the core of the first and second models, respectively. As would be expected, in both models the maximum of σ_z occurs on the root of the groove indicating the notch effect. In the first model, $(\sigma_z)_{max}$ has a value of 54 psi, in the second model, 42 psi. They are less than $(\sigma_f)_{max}$ in both models.

Stress Concentration Factors

We will define stress concentration factors K_z, K_p, and K_s as follows:

$$K_z = (\sigma_f)_{max}/(P/A_z) \qquad (10a)$$

$$K_p = (\sigma_f)_{max}/(P/A_p) \qquad (10b)$$

$$K_s = (\sigma_f)_{max}/(P/A_s) \qquad (10c)$$

where P is the applied load, A_z the narrowest cross sectional area, A_p the shearing area along the pitch circle, and A_s the shearing area along the circle of the groove root. The results are shown in Table I.

TABLE I. STRESS CONCENTRATION FACTORS

	Model 1	Model 2
Loads, Pounds	59.1	58.8
$(\sigma_f)_{max}$, psi	61	98
A_z, sq. in.	$(\pi/4)(2.388)^2$	$(\pi/4)(2.328)^2$
K_z	4.6	7.1
A_p, sq. in.	$\pi(3)(1/2)$	-
K_p	4.9	-
A_s, sq. in.	$\pi(2.388)(1)$	$\pi(2.328)(1)$
K_s	7.7	12.2

Contact Stresses

In the determination of contact stresses, a $n\theta t$ orthogonal coordinate system was used, in which n was the direction perpendicular to the contact, θ the circumferential direction, and t the tangential direction. Equation (5) takes the following form

$$(\sigma_n)_i = (\sigma_n)_o - \sum_o^i (\Delta\tau_{nt}/\Delta t)\Delta n - \sum_o^i (\Delta\tau_{\theta t}/\Delta\theta)\Delta n \qquad (11)$$

Because of axial symmetry, $\tau_{\theta t} \equiv \tau_{\theta n} \equiv 0$, equation (11) reduces to

$$(\sigma_n)_i = (\sigma_n)_o - \sum_{o}^{i} (\Delta\tau_{nt}/\Delta t)\Delta n \qquad (12)$$

where $(\sigma_n)_o$ is the value of σ_n at the starting point, and τ_{nt} is obtained by making photoelastic observations of the meridian slice at normal incidence to the nt-plane. Once $(\sigma_n)_i$ is known, $(\sigma_t)_i$ can be computed from photoelastic relation similar to equation (6). The remaining normal stress σ_θ can be obtained by making photoelastic observations of a sub-slice at normal incidence to the nθ-plane. Again, due to the interest of preserving the meridian slices, the sub-slice has not been prepared and σ_θ has not been determined.

In the first model, contact occurred from A to E, as seen in Figure 8. Contact stresses were determined along lines BB', CC', DD', and EE'. They were perpendicular to AE and were separated from each other by a distance of AE/4. For lines BB', CC', and DD', the summation was started at B', C', and D', respectively, on the free boundary. Line EE' did not reach the free boundary. An auxiliary line D'E', intersected perpendicularly with EE' at E', was employed. The summation along D'E' provided data at E', the starting point for line EE'. Figure 8 shows the distributions of σ_n, σ_t, and τ_{nt} along contact surface AE in the first model. Both σ_n and τ_{nt} reached their maximum value of -60 psi and -28 psi, respectively, at point E.

Contact stresses were also determined along the line EE' in the second model. Figure 9 shows the distribution of σ_n, σ_t, and τ_{nt} along EE'. The maximum compression is given by σ_n at E' (about -180 psi) and is about three times the maximum compression in the first model.

In the first model, the angle between the loaded surface and the horizontal was found to be 7.5 degrees instead of 7 degrees. In the second model, contact occurred at a point making an angle of 40.3 degrees with the vertical instead of 45 degrees. These differences are probably due to the combined effect of tolerance in model manufacturing and deformation.

DISCUSSIONS

Critical Regions

In both models the largest tensile fillet stresses are located at a point away from the narrowest section toward the loaded surface. Table II shows a comparison between $(\sigma_f)_{max}$ and $(\sigma_z)_{max}$.

TABLE II. A COMPARISON BETWEEN $(\sigma_f)_{max}$ AND $(\sigma_z)_{max}$

	Model 1	Model 2
$(\sigma_f)_{max}$, psi largest tensile fillet stress	61 psi, 21° away from the narrowest section, Figure 6(a)	98 psi, 43° away from the narrowest section, Figure 6(b)
$(\sigma_z)_{max}$, psi maximum value of σ_z at the narrowest section	54 psi, Figure 7(a)	42 psi, Figure 7(b)

It can be seen that $(\sigma_f)_{max}$ is the critical stress. Failure will start when $(\sigma_f)_{max}$ reaches the ultimate limit as loads are increased. The critical region is not the narrowest section but rather the region where $(\sigma_f)_{max}$ is found. Moreover, the fact that $(\sigma_f)_{max}$ in the second model (new profile) is 60 percent greater than that in the first model (British standard buttress) clearly indicates that the new profile is weaker than the British standard buttress although $(\sigma_z)_{max}$ is slightly reduced in the new profile.

Checks

Two independent checks were made.

1. The stress distribution of σ_z on the narrowest section was checked by determining the resultant of σ_z on this section and comparing it with the applied axial load. Taking σ_z from the meridian slices, the integrated axial forces were found to be 55.2 and 57.8 pounds compared to an applied load of 59.1 and 58.8 pounds in the first and second models, respectively.

2. The distribution of contact stresses was checked by determining σ_z and its effect on the contact surface, and comparing it with the applied axial load. The stress σ_z was calculated from the usual stress transformation equation. The distribution of σ_z along contact surface in the first model is shown in Figure 8. The integrated axial force was found to be 62.4 pounds compared to an applied load of 59.1 pounds. In the second model, the contact region extended over an arc of 12.5 degrees. Assuming a parabolic distribution of stresses over the contact region, the stress σ_z was calculated and the result was found to be 61.7 pounds compared to an applied load of 58.8 pounds.

Heywood's Empirical Equation

In 1948 Heywood[1] suggested an empirical equation of the following form

$$(\sigma_f)_{max} = [1+0.26(e/R)^{0.7}][(1.5a/e^2) + (0.36/be)^{1/2}(1+0.25 \sin \gamma)](w/t) \quad (13)$$

for calculating the maximum fillet stress at point A, 30 degrees from the point of tangency on the fillet, Figure 10, where w denotes the load, t the thickness, and the dimensions a, b, e, and R, and the angle γ are as shown in the figure.

Comparison of Experimental Results With Those From Heywood's Equation

In the first model, e = 0.326 inch and R = 0.120 inch, the section EA, Figure 8, was equally divided into eight segments. The dimensions a and b, and the angle γ were determined at midpoint of each segment by considering σ_n and τ_{nt} at the point and their geometries. Equation (13) was used to calculate $(\sigma_f)_{max}/(w/t)$ at each point, and $(\sigma_f)_{max}$ due to individual load at each segment was found. The result gave a $(\sigma_f)_{max}$ of 57 psi at 30 degrees in comparison with the experimental result of 61 psi at 62 degrees.

Recently, Allison and Hearn[6] reported the movement of maximum stress position around the fillet as load position varies. They observed a range of angle from 30 degrees to 70 degrees. Based on Allison's results, the summation process is not valid since the stress maxima do not occur at the same position. This has an unfavorable effect of reducing the $(\sigma_f)_{max}$ from its calculated value of 57 psi. Therefore, Heywood's equation is not

---

[1]Heywood, R. B., "Tensile Stresses in Loaded Projections," Proceedings of the Institute of Mechanical Engineers, Vol. 159, pp. 384-391, 1948.

[6]Allison, I. M. and Hearn, E. J., "A New Look at the Bending Strength of Gear Teeth," Experimental Mechanics, Vol. 20, No. 7, pp. 217-225, July 1980.

applicable in our problem. Also, a, b, e, and γ in equation (13) are unknown quantites.

In the second model, equation (13) can not be evaluated due to the 40.3 degree angle of its load position.

CONCLUSIONS

Stresses in single-groove connection were investigated photoelastically by means of the three-dimensional shear-difference method in combination with stress-freezing-and-slicing techniques. Two groove profiles were studied; namely, the British standard buttress and the new profile. The results show that, in both profiles, the maximum fillet stress $(\sigma_f)_{max}$ does not occur at the groove root. Therefore, the narrowest section is not the critical region. Although the stress at the groove root of the new profile is slightly less than that of the British standard buttress, the new profile is weaker than the British standard buttress since the critical stress, $(\sigma_f)_{max}$, in the new profile is 1.6 times of that in the British standard buttress. Stress distributions were also determined across the narrowest section and the contact region. Appropriate checks for the accuracy of the results were made.

Heywood's empirical equation was reviewed. It is concluded that this equation is not applicable in our problem for the following reasons: (a) $(\sigma_f)_{max}$ does not occur at 30 degrees from the point of tangency on the fillet, and (b) the load and its position are unknowns rather than known quantities as shown in the equation.

Further work on multi-groove connections is in progress and will be reported at a later date.

REFERENCES

1. Heywood, R. B., "Tensile Fillet Stresses in Loaded Projections," Proceedings of the Institute of Mechanical Engineers, Vol. 159, pp. 384-391, 1948.
2. Jessop, H. T. and Harris, F. C., "Photoelasticity - Principle and Methods," p. 176, Dover Publications, Inc., New York, 1949.
3. Cheng, Y. F., "Some New Techniques for Scattered Light Photoelasticity," Experimental Mechanics, Vol. 3, No. 11, pp. 275-278, Nov. 1963.
4. Frocht, M. M. and Guernsey, R. Jr., "Studies in Three-Dimensional Photoelasticity - The Application of the Shear-Difference Method to the General Space Problem," Proceedings First US National Congress of Applied Mechanics, pp. 301-307, December 1952.
5. Frocht, M. M. and Guernsey, R. Jr., "Further Work on the General Three-Dimensional Photoelastic Problem," Journal of Applied Mechanics, Trans. ASME, Vol. 77, No. 2, pp. 183-189, June 1955.
6. Allison, I. M. and Hearn, E. J., "A New Look at the Bending Strength of Gear Teeth," Experimental Mechanics, Vol. 20, No. 7, pp. 217-225, July 1980.

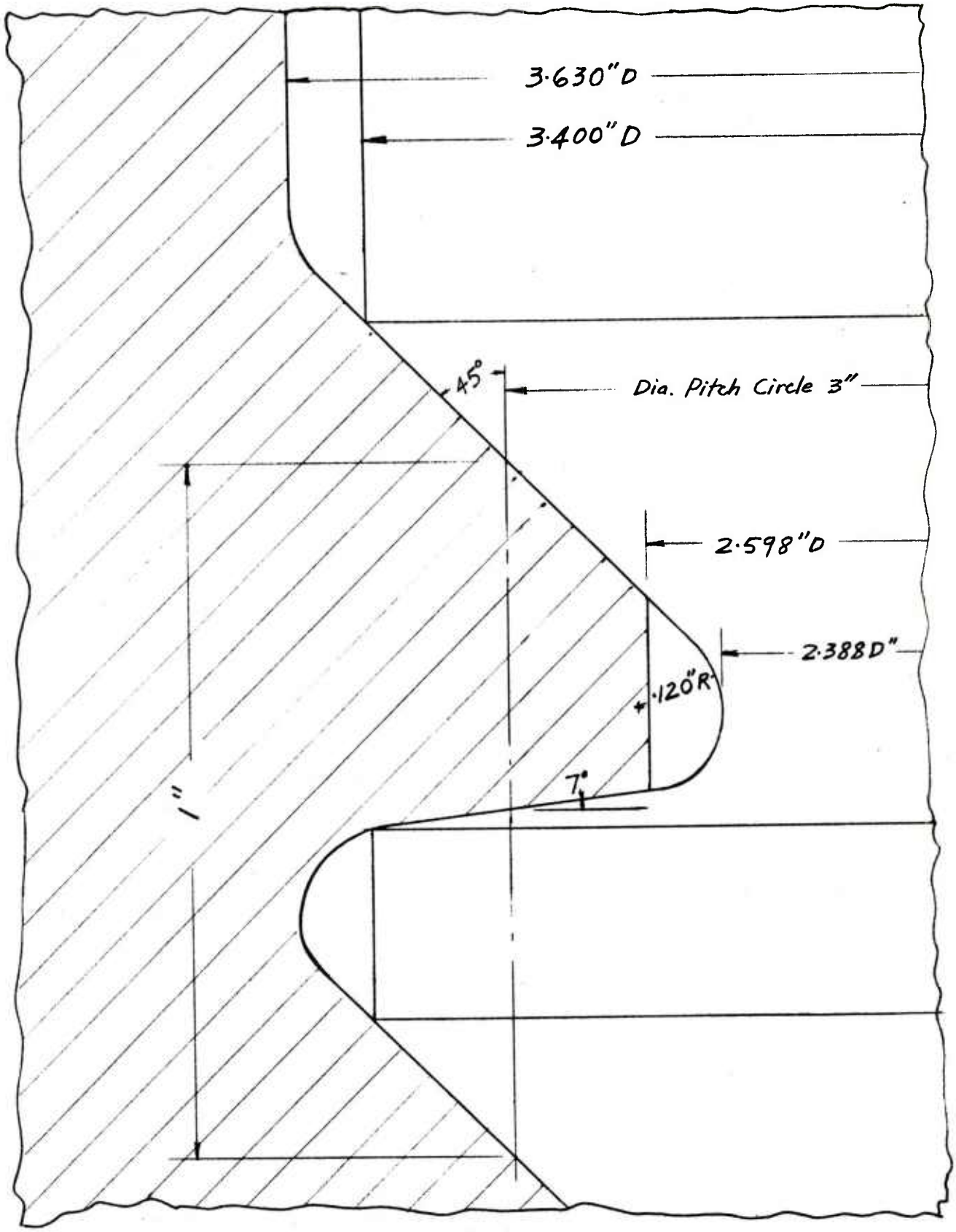

Figure 1. British standard buttress profile

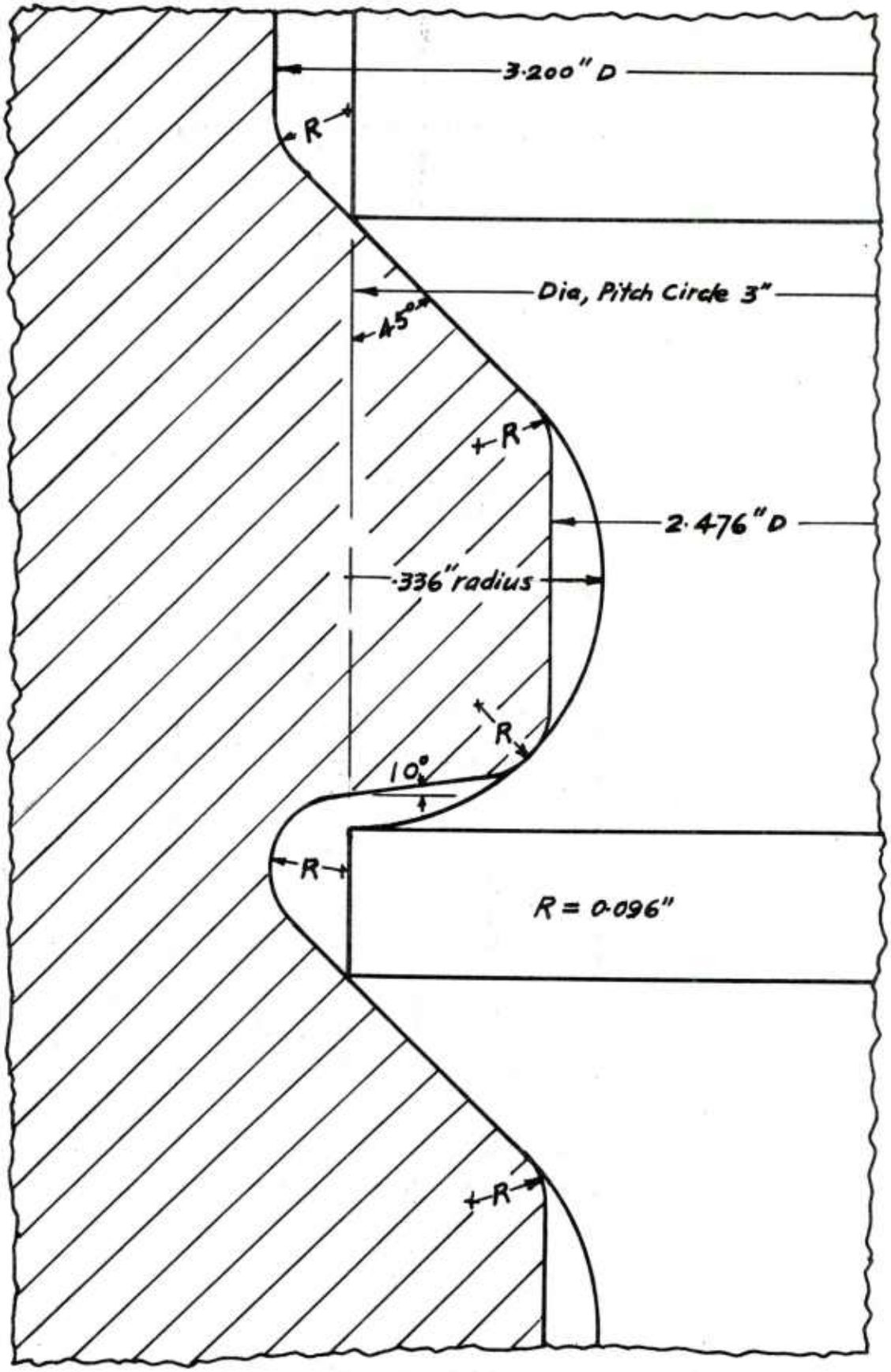

Figure 2. New profile

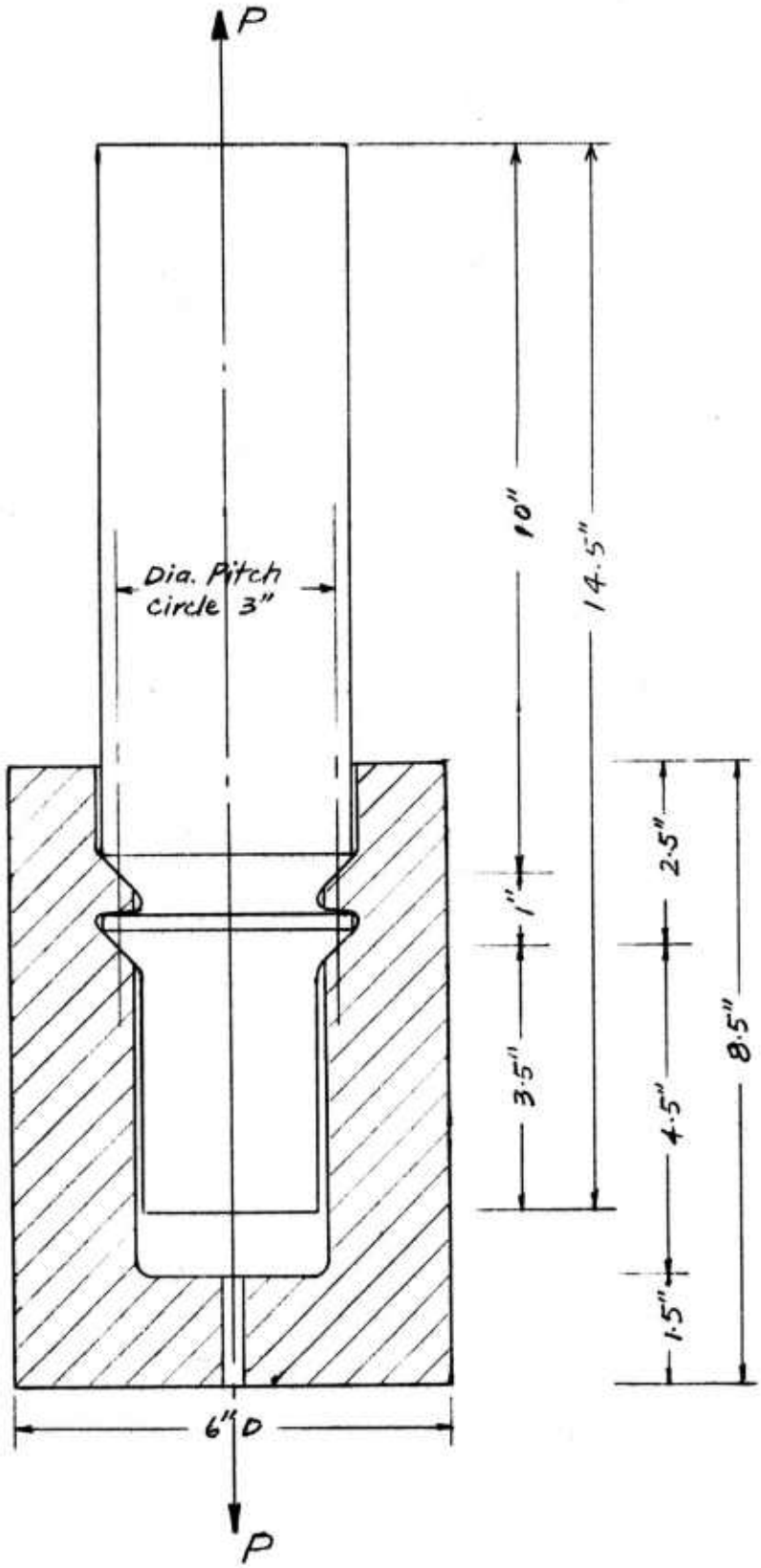

Figure 3. Sketch of the first model

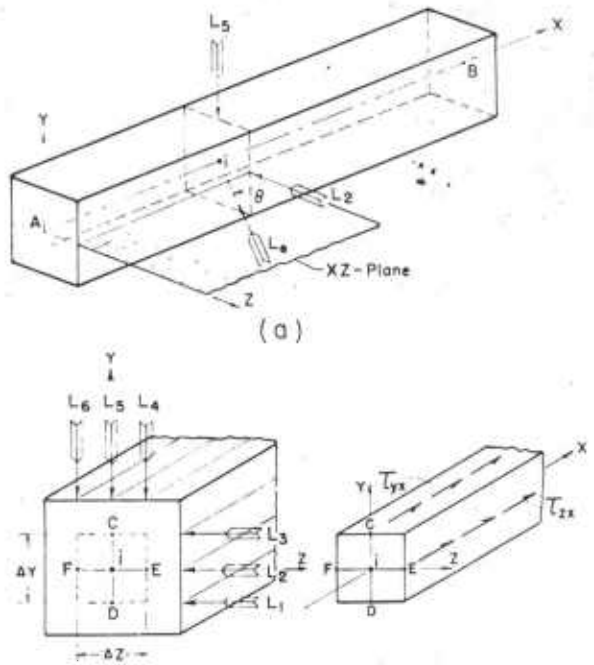

Figure 4. Sketch showing the shear-difference method

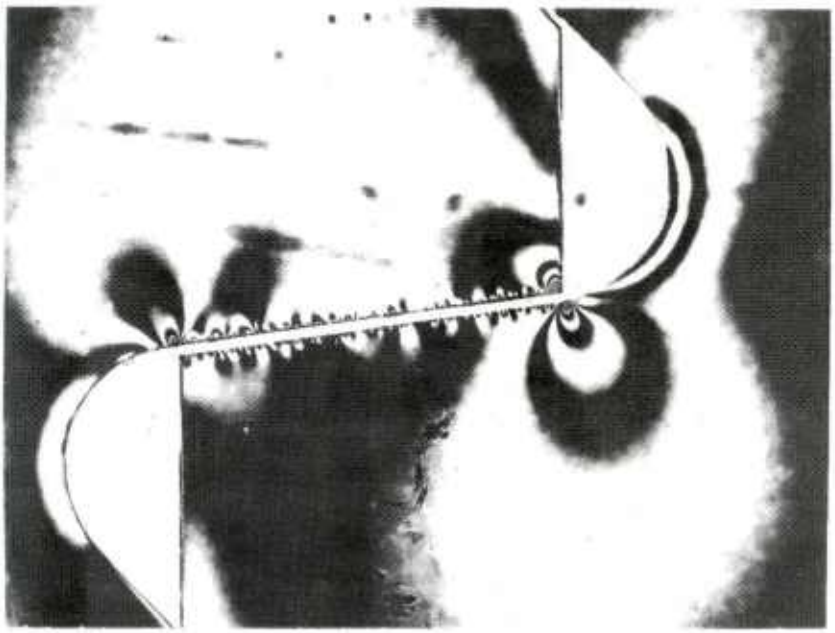

(a) British standard buttress profile

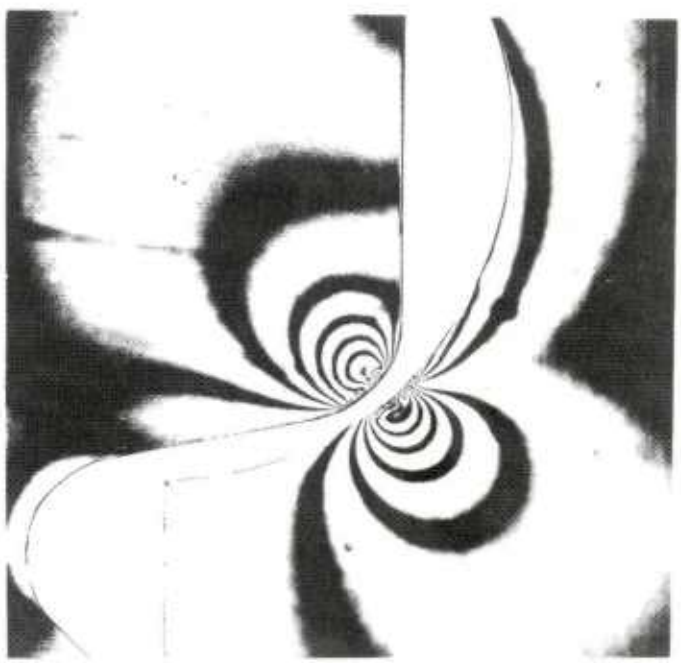

(b) New profile

Figure 5. Photographs of stress patterns

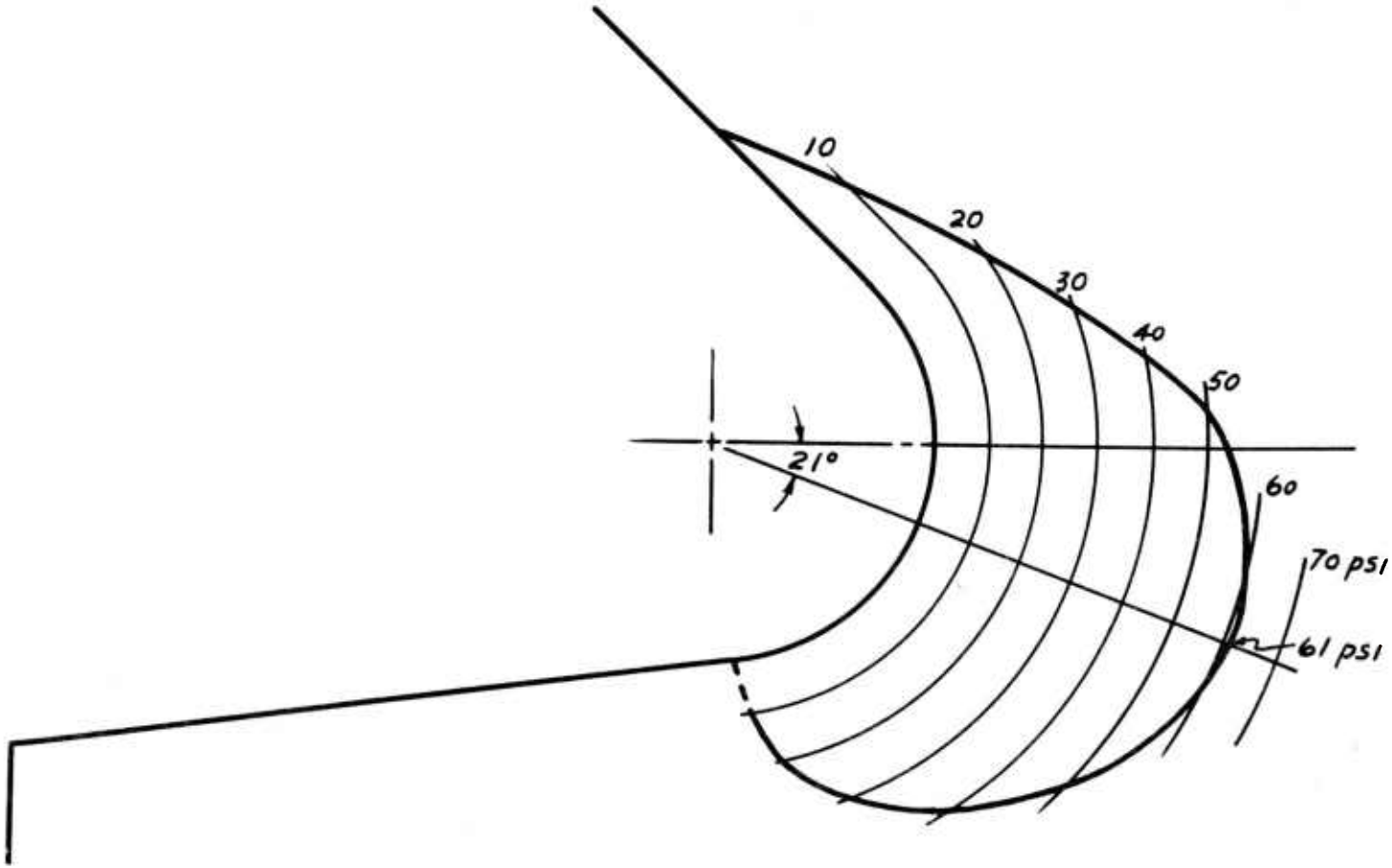

(a) Core of the first model, British standard buttress profile

Figure 6. Distributions of fillet boundary stress

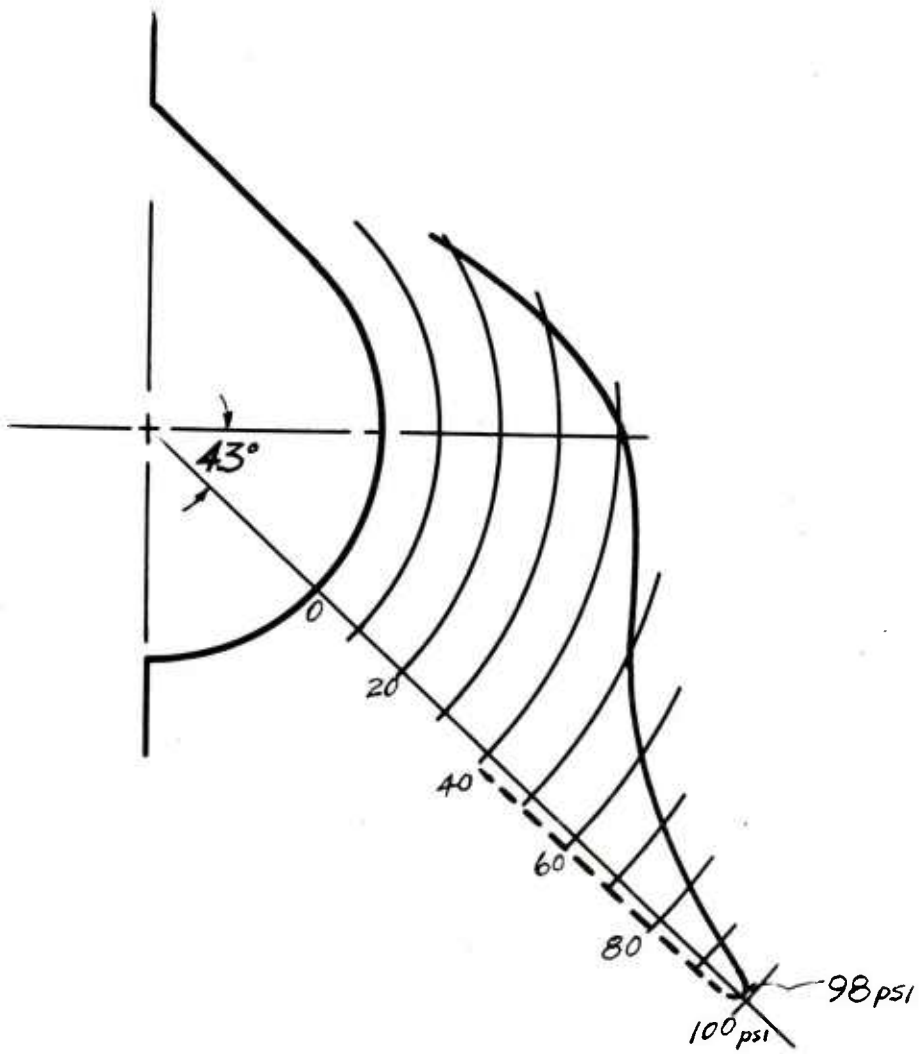

(b) Core of the second model, new profile

Figure 6. Distributions of fillet boundary stress

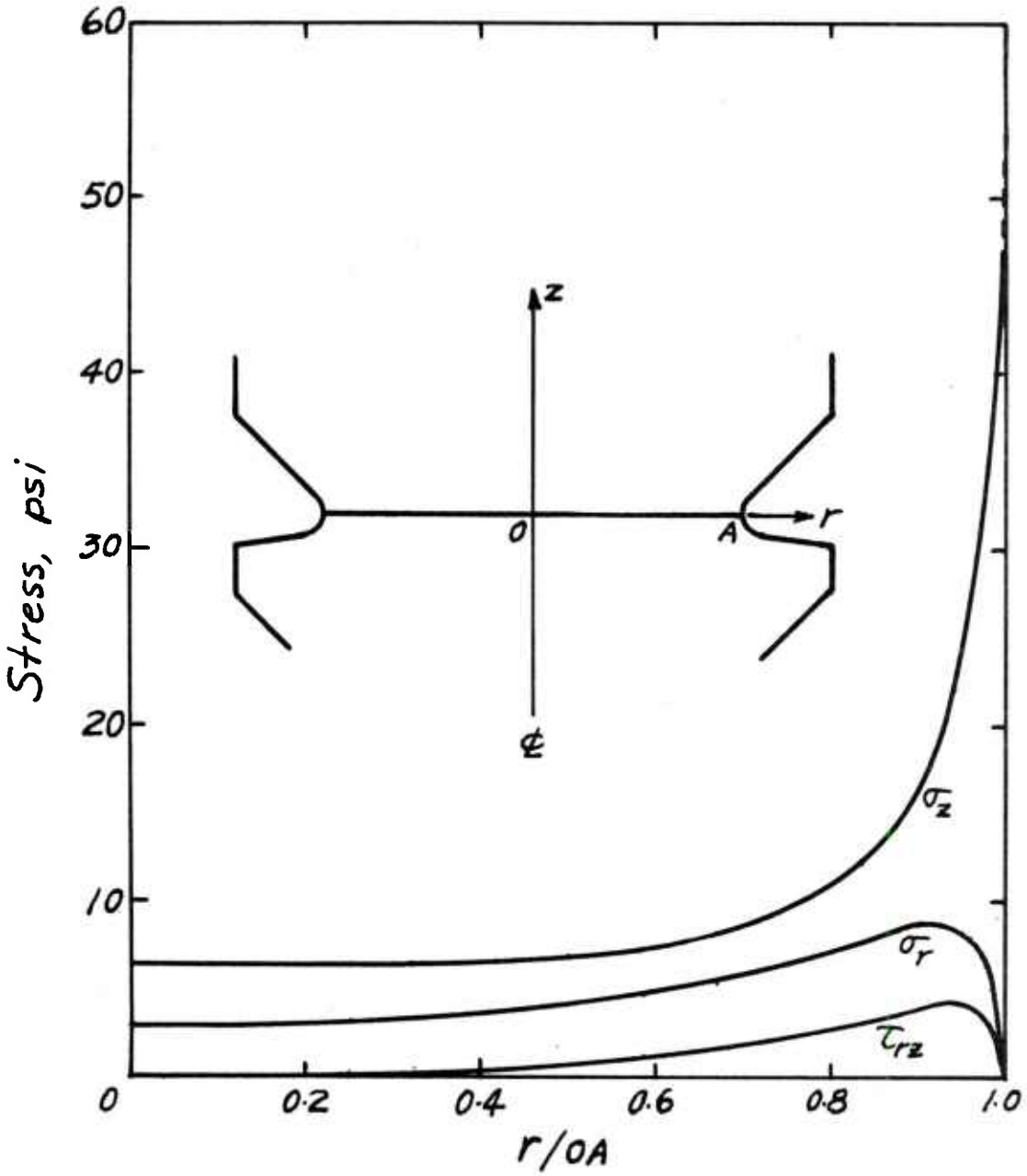

(a) Core of the first model, British standard buttress profile

Figure 7. Distributions of σ_r, σ_z, and τ_{rz} on the narrowest section

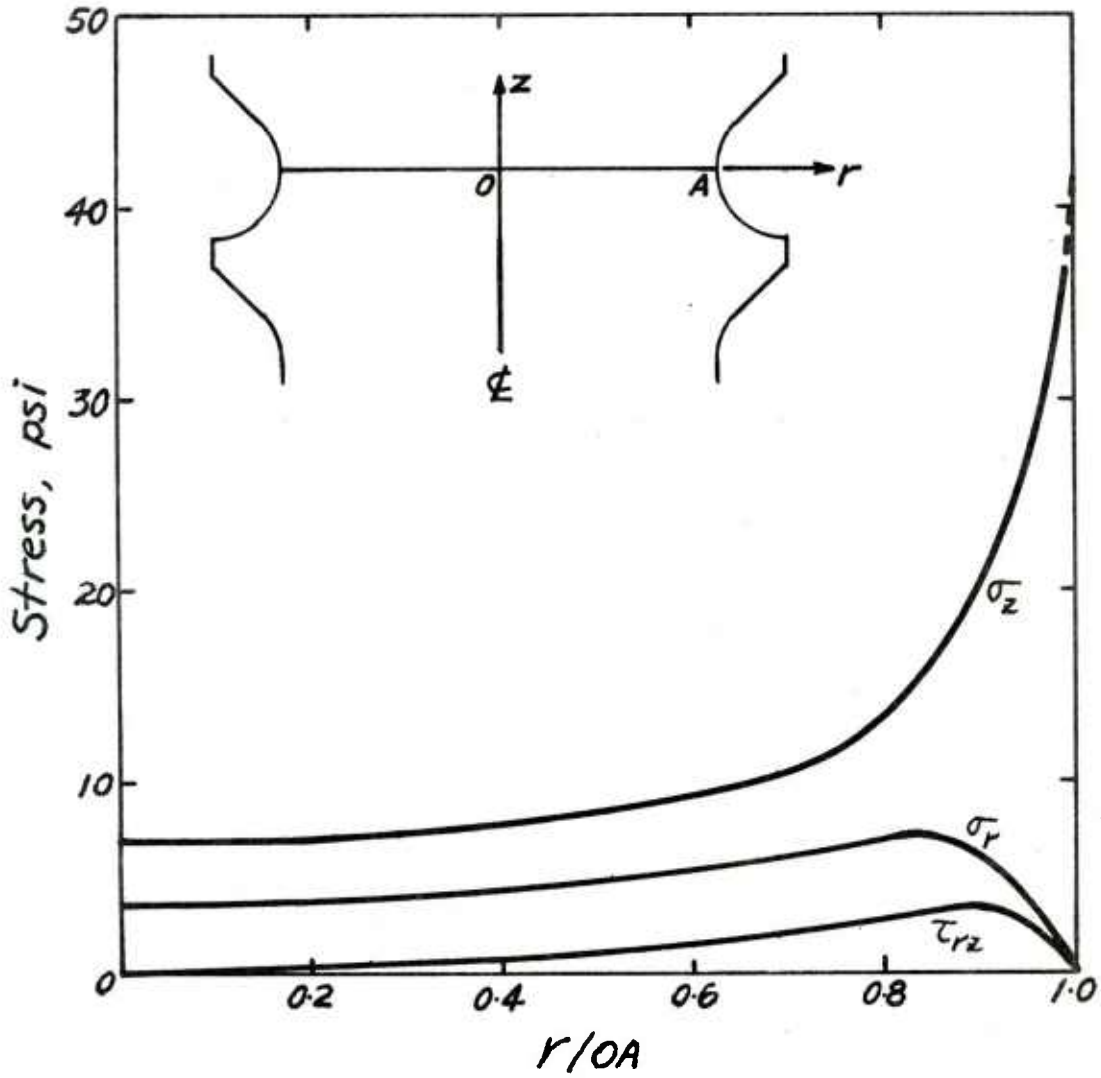

(b) Core of the second model, new profile

Figure 7. Distributions of σ_r, σ_z, and τ_{rz} on the narrowest section

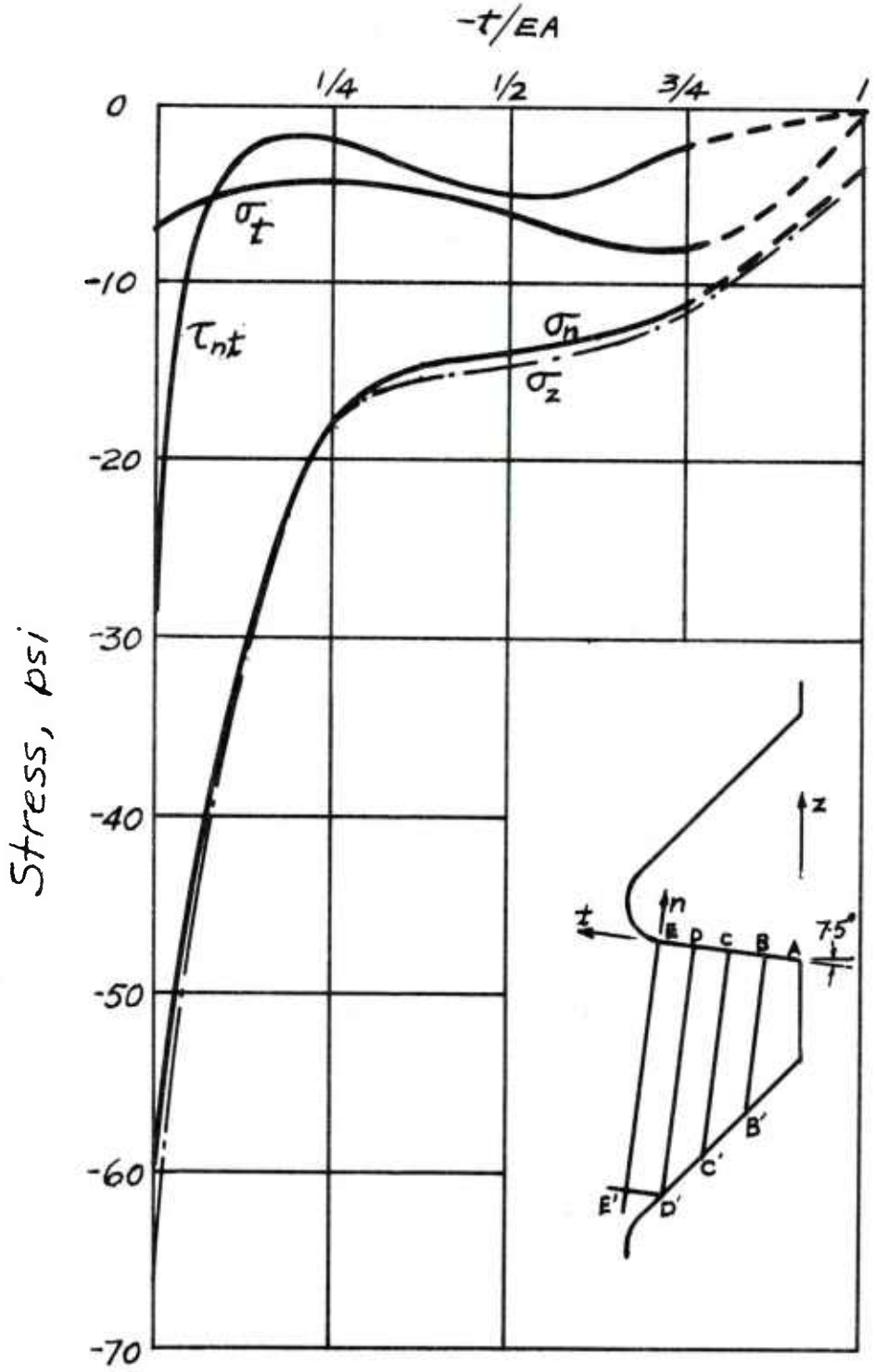

Figure 8. Distributions of σ_n, σ_t, and τ_{nt} on the contact region in the first model

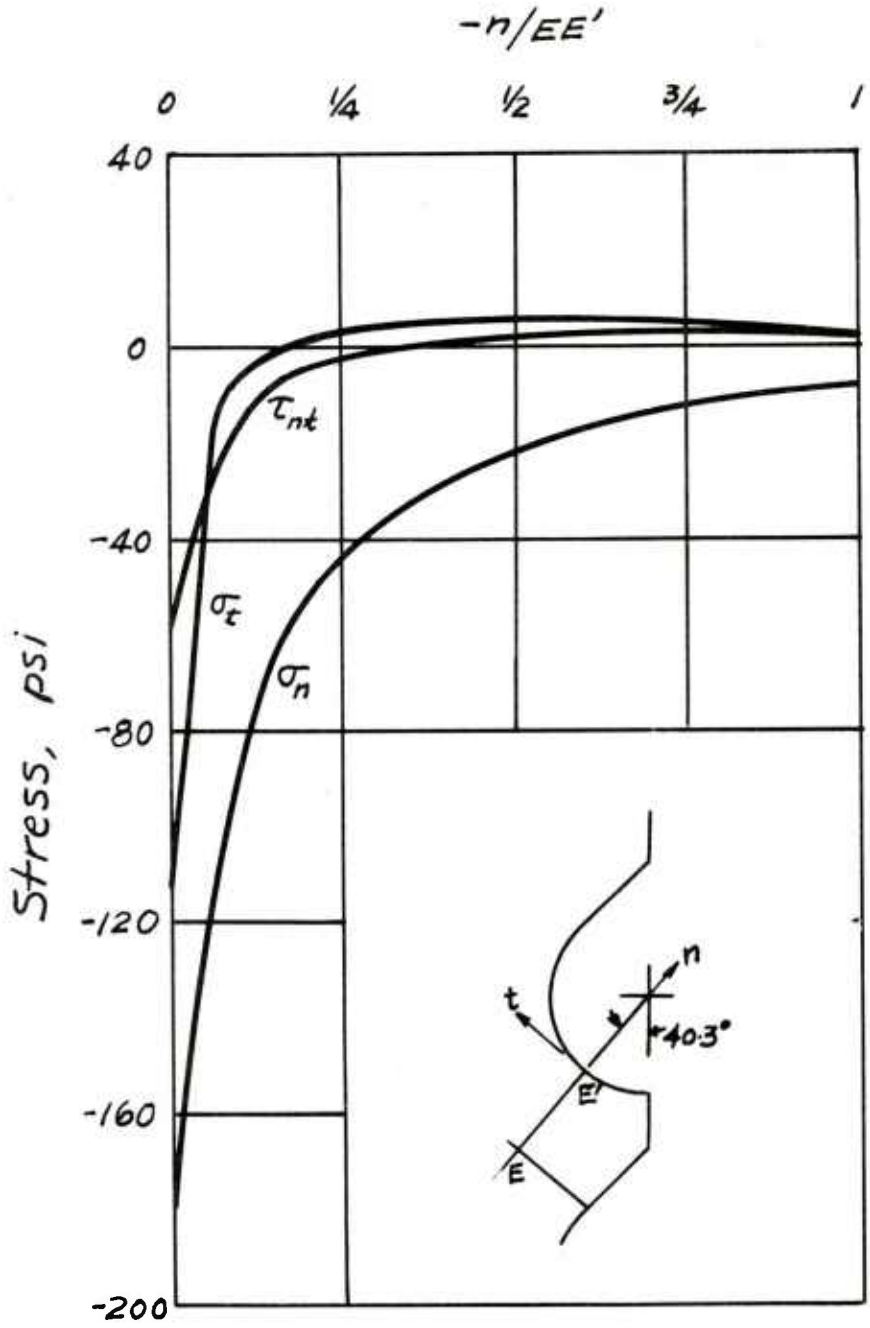

Figure 9. Contact stresses σ_n, σ_t, and τ_{nt} in the second model

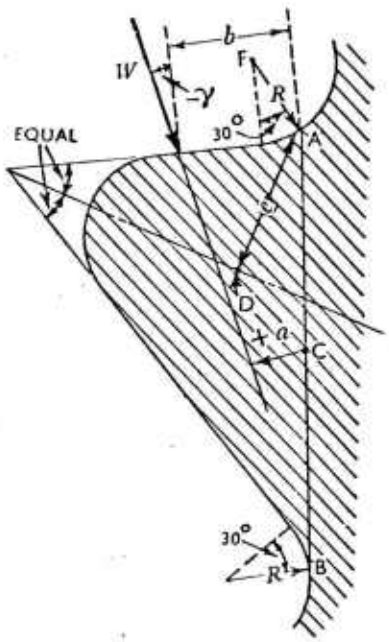

Figure 10. Dimensions used for calculating maximum fillet stress by Heywood

TECHNICAL REPORT INTERNAL DISTRIBUTION LIST

	NO. OF COPIES
COMMANDER	1
CHIEF, DEVELOPMENT ENGINEERING BRANCH	1
ATTN: DRDAR-LCB-DA	1
-DM	1
-DP	1
-DR	1
-DS	1
-DC	1
CHIEF, ENGINEERING SUPPORT BRANCH	1
ATTN: DRDAR-LCB-SE	1
-SA	1
CHIEF, RESEARCH BRANCH	2
ATTN: DRDAR-LCB-RA	1
-RC	1
-RM	1
-RP	1
CHIEF, LWC MORTAR SYS. OFC. ATTN: DRDAR-LCB-M	1
CHIEF, IMP. 81MM MORTAR OFC. ATTN: DRDAR-LCB-I	1
TECHNICAL LIBRARY ATTN: DRDAR-LCB-TL	5
TECHNICAL PUBLICATIONS & EDITING UNIT ATTN: DRDAR-LCB-TL	2
DIRECTOR, OPERATIONS DIRECTORATE	1
DIRECTOR, PROCUREMENT DIRECTORATE	1
DIRECTOR, PRODUCT ASSURANCE DIRECTORATE	1

NOTE: PLEASE NOTIFY ASSOC. DIRECTOR, BENET WEAPONS LABORATORY, ATTN: DRDAR-LCB-TL, OF ANY REQUIRED CHANGES.

TECHNICAL REPORT EXTERNAL DISTRIBUTION LIST

	NO. OF COPIES
ASST SEC OF THE ARMY RESEARCH & DEVELOPMENT ATTN: DEP FOR SCI & TECH THE PENTAGON WASHINGTON, D.C. 20315	1
COMMANDER US ARMY MAT DEV & READ. COMD ATTN: DRCDE 5001 EISENHOWER AVE ALEXANDRIA, VA 22333	1
COMMANDER US ARMY ARRADCOM ATTN: DRDAR-LC	1
-ICA (PLASTICS TECH EVAL CEN)	1
-LCE	1
-LCM	1
-LCS	1
-LCW	1
-TSS(STINFO) DOVER, NJ 07801	2
COMMANDER US ARMY ARRCOM ATTN: DRSAR-LEP-L ROCK ISLAND ARSENAL ROCK ISLAND, IL 61299	1
DIRECTOR US Army Ballistic Research Laboratory ATTN: DRDAR-TSB-S (STINFO) ABERDEEN PROVING GROUND, MD 21005	1
COMMANDER US ARMY ELECTRONICS COMD ATTN: TECH LIB FT MONMOUTH, NJ 07703	1
COMMANDER US ARMY MOBILITY EQUIP R&D COMD ATTN: TECH LIB FT BELVOIR, VA 22060	1
COMMANDER US ARMY TANK-AUTMV R&D COMD ATTN: TECH LIB - DRDTA-UL	1
MAT LAB - DRDTA-RK WARREN MICHIGAN 48090	1
COMMANDER US MILITARY ACADEMY ATTN: CHMN, MECH ENGR DEPT WEST POINT, NY 10996	1
COMMANDER REDSTONE ARSENAL ATTN: DRSMI-RB	2
-RRS	1
-RSM ALABAMA 35809	1
COMMANDER ROCK ISLAND ARSENAL ATTN: SARRI-ENM (MAT SCI DIV) ROCK ISLAND, IL 61202	1
COMMANDER HQ, US ARMY AVN SCH ATTN: OFC OF THE LIBRARIAN FT RUCKER, ALABAMA 36362	1
COMMANDER US ARMY FGN SCIENCE & TECH CEN ATTN: DRXST-SD 220 7TH STREET, N.E. CHARLOTTESVILLE, VA 22901	1
COMMANDER US ARMY MATERIALS & MECHANICS RESEARCH CENTER ATTN: TECH LIB - DRXMR-PL WATERTOWN, MASS 02172	2

NOTE: PLEASE NOTIFY COMMANDER, ARRADCOM, ATTN: BENET WEAPONS LABORATORY, DRDAR-LCB-TL, WATERVLIET ARSENAL, WATERVLIET, N.Y. 12189, OF ANY REQUIRED CHANGES.

TECHNICAL REPORT EXTERNAL DISTRIBUTION LIST (CONT)

	NO. OF COPIES
COMMANDER US ARMY RESEARCH OFFICE P.O. BOX 12211 RESEARCH TRIANGLE PARK, NC 27709	1
COMMANDER US ARMY HARRY DIAMOND LAB ATTN: TECH LIB 2800 POWDER MILL ROAD ADELPHIA, MD 20783	1
DIRECTOR US ARMY INDUSTRIAL BASE ENG ACT ATTN: DRXPE-MT ROCK ISLAND, IL 61201	1
CHIEF, MATERIALS BRANCH US ARMY R&S GROUP, EUR BOX 65, FPO N.Y. 09510	1
COMMANDER NAVAL SURFACE WEAPONS CEN ATTN: CHIEF, MAT SCIENCE DIV DAHLGREN, VA 22448	1
DIRECTOR US NAVAL RESEARCH LAB ATTN: DIR, MECH DIV CODE 26-27 (DOC LIB) WASHINGTON, D. C. 20375	1 1
NASA SCIENTIFIC & TECH INFO FAC. P. O. BOX 8757, ATTN: ACQ BR BALTIMORE/WASHINGTON INTL AIRPORT MARYLAND 21240	1

	NO. OF COPIES
COMMANDER DEFENSE TECHNICAL INFO CENTER ATTN: DTIA-TCA CAMERON STATION ALEXANDRIA, VA 22314	12
METALS & CERAMICS INFO CEN BATTELLE COLUMBUS LAB 505 KING AVE COLUMBUS, OHIO 43201	1
MECHANICAL PROPERTIES DATA CTR BATTELLE COLUMBUS LAB 505 KING AVE COLUMBUS, OHIO 43201	1
MATERIEL SYSTEMS ANALYSIS ACTV ATTN: DRXSY-MP ABERDEEN PROVING GROUND MARYLAND 21005	1

NOTE: PLEASE NOTIFY COMMANDER, ARRADCOM, ATTN: BENET WEAPONS LABORATORY, DRDAR-LCB-TL, WATERVLIET ARSENAL, WATERVLIET, N.Y. 12189, OF ANY REQUIRED CHANGES.